Geophysical Research Letters

RESEARCH LETTER
10.1029/2019GL086759

Evolution of Denmark Strait Overflow Cyclones and Their Relationship to Overflow Surges

M. Almansi[1], T. W. N. Haine[1], R. Gelderloos[1], and R. S. Pickart[2]

[1]Department of Earth and Planetary Sciences, The Johns Hopkins University, Baltimore, MD, USA, [2]Woods Hole Oceanographic Institution, Woods Hole, MA, USA

Key Points:
- High-transport events associated with the Denmark Strait overflow (DSO) evolve into DSO cyclones downstream
- The underlying dynamics of the DSO cyclones differ between two different types of high-transport events
- The potential vorticity of DSO cyclones is only materially conserved during their growth phase

Supporting Information:
- Supporting Information S1
- Figure S1

Correspondence to:
M. Almansi,
mattia.almansi@jhu.edu

Citation:
Almansi, M., Haine, T. W. N., Gelderloos, R., & Pickart, R. S. (2020). Evolution of Denmark Strait overflow cyclones and their relationship to overflow surges. *Geophysical Research Letters*, *47*, e2019GL086759. https://doi.org/10.1029/2019GL086759

Received 21 OCT 2019
Accepted 3 FEB 2020
Accepted article online 6 FEB 2020

Abstract Mesoscale features present at the Denmark Strait sill regularly enhance the volume transport of the Denmark Strait overflow (DSO). They are important for the Atlantic Meridional Overturning Circulation and ultimately, for the global climate system. Using a realistic numerical model, we find new evidence of the causal relationship between overflow surges (i.e., mesoscale features associated with high-transport events) and DSO cyclones observed downstream. Most of the cyclones form at the Denmark Strait sill during overflow surges and, because of potential vorticity conservation and stretching of the water column, grow as they move equatorward. A fraction of the cyclones form downstream of the sill, when anticyclonic vortices formed during high-transport events start collapsing. Regardless of their formation mechanism, DSO cyclones weaken starting roughly 150 km downstream of the sill, and potential vorticity is only materially conserved during the growth phase.

Plain Language Summary Ocean currents affecting the global climate are sustained by cold and dense water that sinks in the North Atlantic Ocean. A large portion of this water passes through Denmark Strait, the ocean channel located between Greenland and Iceland. The amount of water entering the strait varies from day to day and is controlled by ocean vortices. Knowing the mechanisms associated with these vortices is of key importance for understanding and predicting Earth's climate. Using a realistic numerical model, we find that the vortices are generated in the strait during dense water surges. In one scenario, the ocean vortices cross Denmark Strait rotating in the same direction as the Earth (counterclockwise). These vortices strengthen as they move toward the south. If the vortices initially rotate clockwise, they move slowly and quickly collapse. The water converging south of them triggers the formation of new vortices rotating counterclockwise. All of these energetic vortices move toward the equator. First they quickly grow, then they lose energy starting roughly 150 km south of Denmark Strait.

1. Introduction

Denmark Strait is an ocean channel located between Greenland and Iceland (Figure 1a). It is a gateway between the Nordic Seas and the subpolar North Atlantic. The Denmark Strait overflow (DSO) is a bottom-trapped current transporting dense water equatorward. After crossing Denmark Strait, the DSO volume flux (transport) increases rapidly by entrainment (Dickson & Brown, 1994) and supports the Atlantic Meridional Overturning Circulation (AMOC). The East Greenland Current system (EGC), which involves two separate branches (Våge et al., 2013), flows southward along the East Greenland coast and contributes about two thirds of the DSO transport at the sill (Harden et al., 2016). The remaining third of DSO water is transported primarily by the North Icelandic Jet (NIJ; Jonsson & Valdimarsson, 2004, Semper et al., 2019), which flows toward Denmark Strait along the north side of Iceland. The poleward flowing North Icelandic Irminger Current (NIIC) is another contributor to the DSO water (Mastropole et al., 2017).

Studies on the DSO transport have found no long-term trends (Jochumsen et al., 2012, 2017). Observations and numerical models show a pronounced high-frequency variability (from 1 day to 1 week at the sill; Haine, 2010; Macrander et al., 2007; Ross, 1984; von Appen et al., 2017). Cooper (1955) characterized thick lenses of overflow water associated with high volume fluxes known as "boluses," and Mastropole et al. (2017) found boluses in about 40% of a 20-year collection of shipboard measurements. "Pulses" are another dominant mesoscale feature occurring approximately every 5 days at the Denmark Strait sill. They are associated with a thinning and acceleration of the DSO layer (von Appen et al., 2017). Boluses and pulses are overflow surges augmenting the yearly mean transport of the DSO by about 30% (Almansi et al., 2017). Moritz et al.

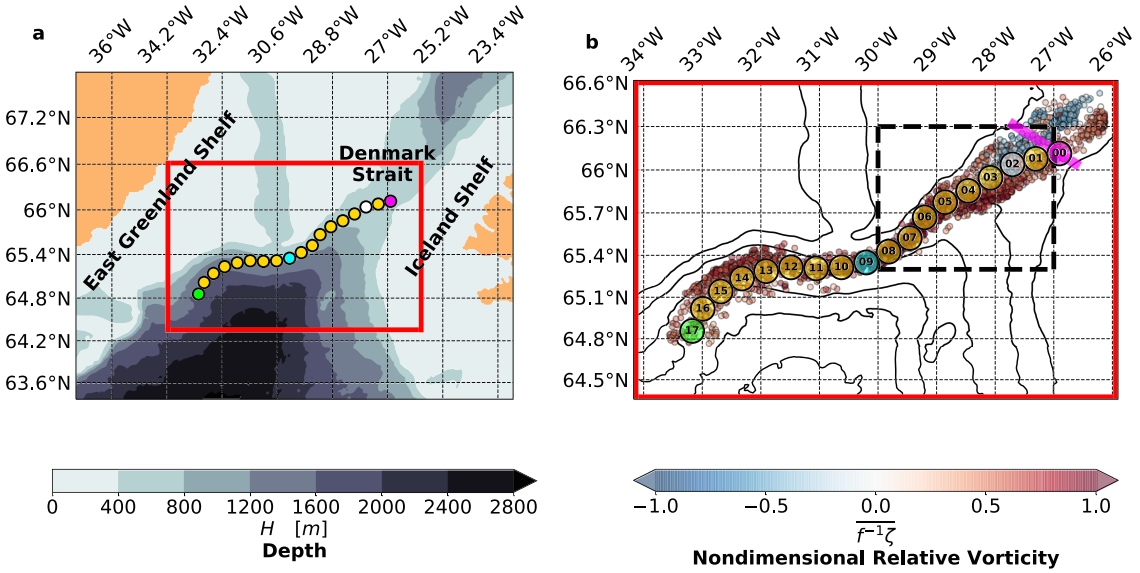

Figure 1. (a) Seafloor bathymetry in the region of interest for this study. Red lines bound the area fed to the vortex detection algorithm. (b) Location of the centers of the detected vortices color coded by their mean nondimensional relative vorticity ($\overline{f^{-1}\zeta}$) at a depth of $5H/8$. Black contours show the bathymetry (same interval used in a). Black dashed lines bound the region shown in Figure 3. Circles indicate the stations along the DSO path (Koszalka et al., 2017). Circles colored in magenta, white, blue, and green indicate where the DSO path crosses hydrographic sections known as the Látrabjarg Line (LL; magenta line), Denmark Strait South (DSS), Transient Tracers in the Ocean (TTO), and Spill Jet (SJ), respectively.

(2019) found that high-transport events at the sill occasionally correspond to anticyclonic eddies. Spall et al. (2019) characterized a third type of mesoscale feature referred to as "flooding events." During these events, the NIIC migrates westward, and the deepest part of the sill is filled with subtropical-origin water. Boluses, pulses, and flooding events are all associated with the meandering of the hydrographic front in Denmark Strait (Spall et al., 2019).

Downstream of Denmark Strait, the high-frequency variability of the overflow is dominated by the presence of energetic features known as "DSO cyclones." The first studies of these features used laboratory experiments (Whitehead et al., 1990), satellite imagery (Bruce, 1995), and surface drifter trajectories (Krauss, 1996) to describe their basic characteristics. Several studies then explored the underlying dynamics of the cyclones (Jungclaus et al., 2001; Krauss & Käse, 1998; Reszka et al., 2002; Spall & Price, 1998; Shi et al., 2001). Spall and Price (1998) formulated the so called "PV Outflow Hypothesis." Cyclogenesis in their three-layer model was explained via conservation of potential vorticity (PV) in the presence of strong vortex stretching. von Appen et al. (2014) found that DSO cyclones represent the largest source of variability roughly 300 km downstream of Denmark Strait. Although the model results of Spall and Price (1998) indicate that these features can form from a steady overflow, von Appen et al. (2017) hypothesized a one-to-one connection between the passage of boluses/pulses and the formation of DSO cyclones.

Characterizing the DSO high-frequency fluctuations is of key importance for understanding and predicting the AMOC variability. At present, the notion of a causal relationship between the mesoscale variability at the sill and the downstream cyclones remains a hypothesis that needs to be investigated further. In this paper, we present new evidence for the existence of this relationship. We also investigate how different types of high-transport events trigger the formation of DSO cyclones and describe their evolution along the DSO path.

2. Materials and Methods

2.1. Numerical Circulation Model

We fill the gaps in the sparse measurements along the DSO path using a yearlong, high-resolution, realistic circulation model. The dynamics are simulated using the Massachusetts Institute of Technology General Circulation Model (MITgcm; Marshall et al., 1997). An identical configuration with different atmospheric forcing is described in detail in Almansi et al. (2017). The numerical solutions have been stored at 6-hr frequency and are publicly available on SciServer (Medvedev et al., 2016). The additional fields shown in

this paper can be reproduced using OceanSpy v0.1 (Almansi et al., 2019). The model is particularly well suited to study mesoscale features occurring on short time scales (1–10 days; Almansi et al., 2017; Spall et al., 2019). Haine et al. (2009) found that the spatial resolution of the atmospheric fields used to force high-resolution models significantly affects the ocean circulation in Denmark Strait. Therefore, we use the 15-km resolution Arctic System Reanalysis (ASRv2; Bromwich et al., 2018), which represents a significant improvement (Bromwich et al., 2016) in horizontal resolution of the atmospheric forcing previously implemented (ERA-Interim; Dee et al., 2011). The model solutions have been also compared to data collected upstream of Denmark Strait by Håvik et al. (2019). Vertical sections of hydrographic and velocity fields are consistent with the validation performed by Almansi et al. (2017). Overall, the agreement between the model and the available observations around Denmark Strait is excellent.

2.2. Detection of Mesoscale Features

High-transport events and DSO cyclones are detected independently. Boluses and pulses are identified at the Látrabjarg Line (Figure 1b) using the same criteria as Almansi et al. (2017): Snapshots where the cross-sectional volume flux of the overflow is lower than the yearly 25th percentile are excluded, then the remaining snapshots are deemed to contain a bolus (pulse) if the cross-sectional area covered by the overflow is larger (smaller) than the yearly 65th (35th) percentile. In line with previous studies, the DSO interface corresponds to the isopycnal $\sigma_\theta = 27.8\ \mathrm{kg\ m^{-3}}$ ($\sigma_\theta = \rho - 1,\ 000\ \mathrm{kg\ m^{-3}}$; Dickson & Brown, 1994). DSO cyclones are detected using an automatic vortex detection scheme based on the Okubo-Weiss parameter (OW; Okubo, 1970; Weiss, 1991). The algorithm operates on terrain-following levels (σ-levels) located in the bottom half of the water column and isolates mesoscale features with relative vorticity higher than the strain (see the supporting information for more details). The relative vorticity is defined by $\zeta = \frac{\partial v}{\partial x} - \frac{\partial u}{\partial y}$, where $\mathbf{u} = (u, v, w)$ is the vector velocity field written as a function of Cartesian position $x\hat{\mathbf{x}} + y\mathbf{y} + z\hat{\mathbf{z}}$. The detection algorithm locates vortices with vertical coherence between the σ-levels at a depth of $H/2$ and $3H/4$, where H is the seafloor depth. Hereafter, the fields extracted along terrain-following levels refer to the σ-level at a depth of $5H/8$. Figure 1b shows the location of the centers of the vortices detected. Although the vertical component of the Coriolis parameter (f) does not change significantly within the study region, we present and discuss the nondimensional relative vorticity ($f^{-1}\zeta$). The cyclones ($\overline{f^{-1}\zeta} > 0$; overline indicates a spatial average in the region occupied by the vortex) are located in proximity to the DSO path and move southward along the continental slope. The anticyclones ($\overline{f^{-1}\zeta} < 0$), which are thought to be related to a fraction of DSO cyclones observed at the Spill Jet section (Station #17 in Figure 1b; von Appen et al., 2017), are located on the western side of the Denmark Strait trough.

3. Results

3.1. Relationship Between DSO Cyclones and Overflow Surges

Boluses are coupled with the cyclones detected near the Denmark Strait sill, whereas pulses are coupled with the anticyclones. Specifically, more than 70% of the cyclones (anticyclones) near Station #00 in Figure 1b occur within 48 hr of a bolus (pulse). The temporal distribution of the cyclones and anticyclones detected near the Látrabjarg Line station are consistent with the statistics of boluses and pulses, respectively (Figures 2a and 2b). The variability of overflow surges in the annual cycle simulated is discussed in more detail by Almansi et al. (2017). More than 50% of the boluses and cyclones occurs between March 2008 and August 2008 (Figure 2a), while the frequency of occurrence of pulses and anticyclones is low in spring 2008 (Figure 2b). The distribution of boluses matches very well the frequency of occurrence of the cyclones in all seasons, whereas some biases exist between the seasonal distribution of pulses and anticyclones. Specifically, a lower fraction of anticyclones was detected between September 2007 and November 2007 compared to the pulse events. Nevertheless, the distribution of pulses across the year matches the frequency of occurrence of the anticyclones reasonably well (particularly from December 2007 to August 2008).

Composite vertical sections of the cyclones (Figures 2c, 2e, and 2g) and anticyclones (Figures 2d, 2f, and 2h) at the Látrabjarg Line support the existence of a causal relation with overflow surges. During cyclones, the water near the eastern side of the trough is denser compared to the yearly average (Figure 2c), while it is lighter during anticyclones (Figure 2d). Denser (lighter) water is the result of the shoaling (deepening) of the DSO interface characteristic of boluses (pulses). During anticyclones, the enhanced equatorward flow is confined to the deepest part of the trough (Figure 2f), whereas during cyclones it extends throughout the whole water column. In the latter case, the strongest velocity anomalies are located at the interface

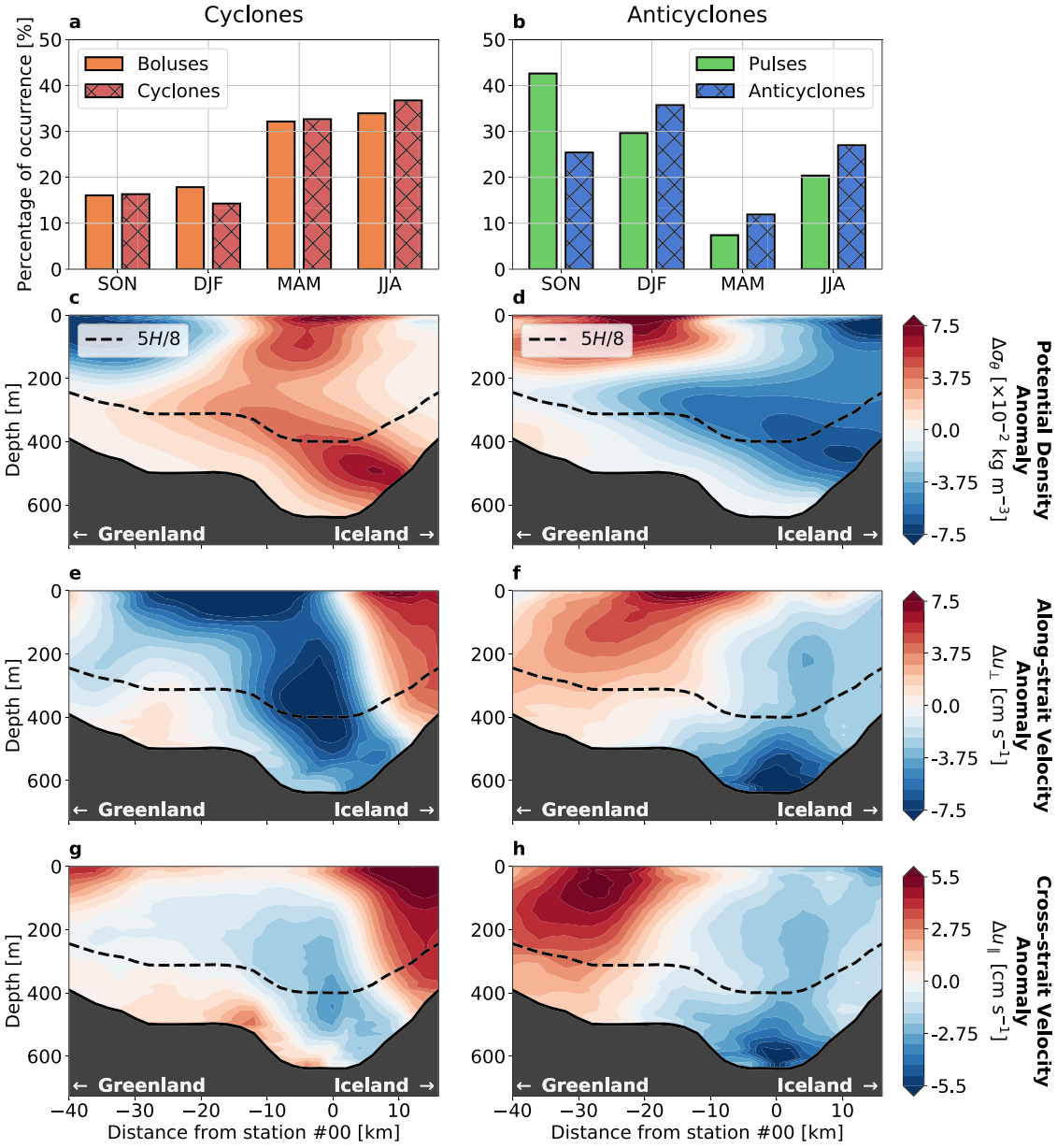

Figure 2. Seasonal frequency of occurrence of (a) boluses/cyclones, and (b) pulses/anticyclones detected near Station #00 (see Figure 1). Percentages represent the number of features detected in a season compared to the total number of features of the same type. Composite vertical sections along the Látrabjarg Line of cyclones (anticyclones) detected within 48 hr from overflow surges minus the yearly averages are shown in the left (right) column: (c and d) potential density; (e and f) along-strait (orthogonal to the LL) velocity; (g and h) cross-strait (tangential to the LL) velocity. The viewer is looking to the north: Positive along-strait (cross-strait) velocities are toward the pole (Iceland). The dashed line corresponds to the σ-level at a depth of $5H/8$.

of the overflow layer (Figure 2e). On the Iceland shelf, the poleward flow of the NIIC strengthens during cyclones (Figure 2e). Finally, anticyclones coincide with an enhanced cross-sectional flow toward Greenland within the overflow layer (Figure 2h). All of these anomalies in the composites of cyclones and anticyclones are consistent with the anomalies associated with boluses and pulses, respectively (Almansi et al., 2017; Mastropole et al., 2017; von Appen et al., 2017).

It has been previously shown that mesoscale features associated with high-transport events act to relax the NIIC hydrographic front in the model (i.e., they are the product of baroclinic instability; Spall et al., 2019). The location of the detected cyclones (Figure 1b) and the front in the along-strait velocity anomalies (Figure 2e) indicate that the cyclones are centered on the eastern side of the trough. The front intersects the whole water column, is located between equatorward anomalies at the center of the trough and poleward

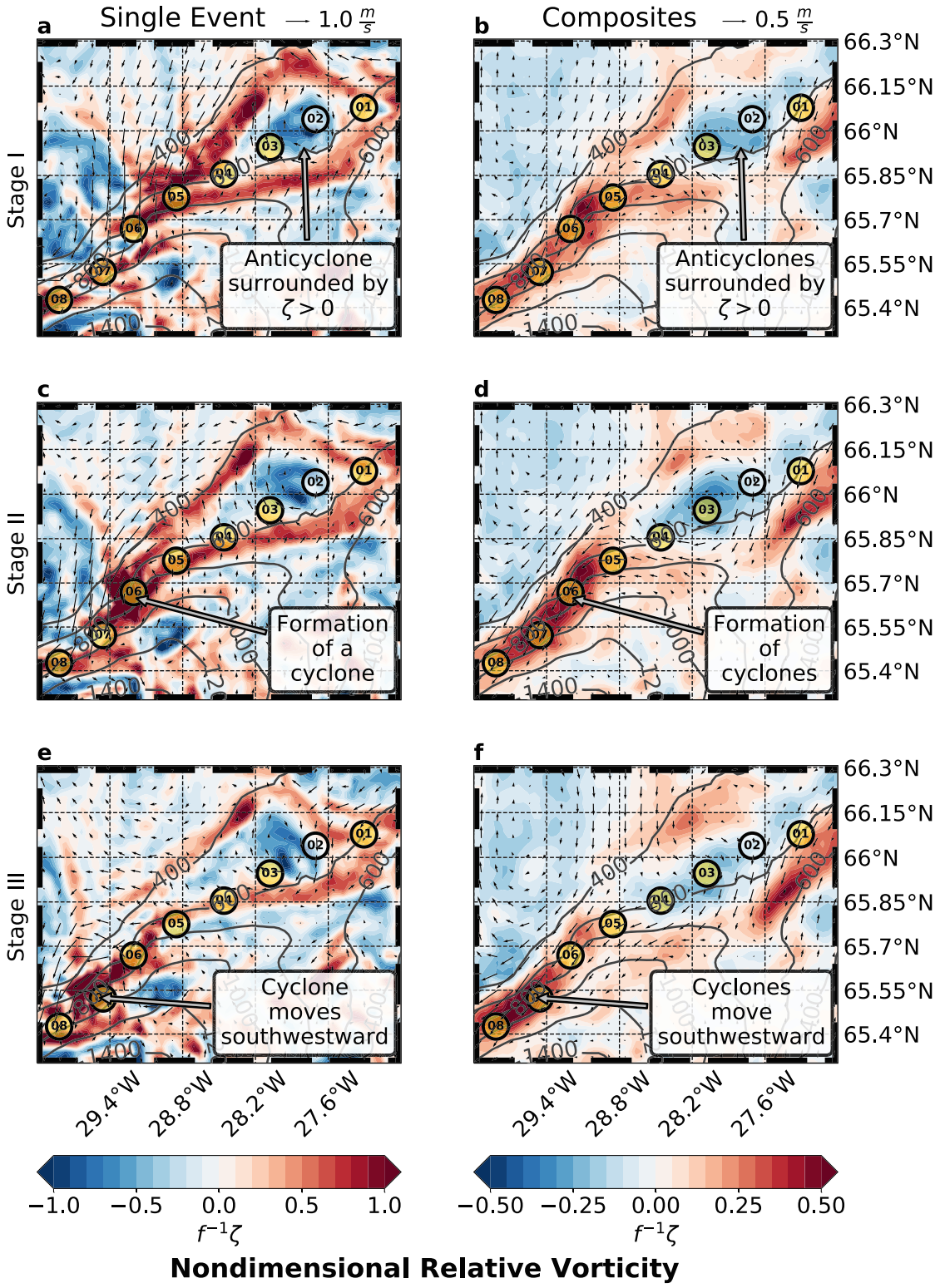

Figure 3. Nondimensional relative vorticity ($f^{-1}\zeta$) and velocity vectors extracted along the σ-level at a depth of $5H/8$. The region shown is bounded by black dashed lines in Figure 1b. Labeled circles correspond to the DSO stations. Three consecutive snapshots (a, c, and e) and composites of 30 anticyclonic events (b, d, and f) are shown. The composite of Stage II (d) includes the snapshots where anticyclones have been detected near Station #03. The stages are 6 hr apart. Dark gray contours indicate the seafloor depth in meters.

anomalies on the eastern side, and is more pronounced at middepths (including the σ-level at a depth of $5H/8$; Figure 2e). As the cyclones move downstream following the DSO path (southwestward), their relative vorticity grows. The height of the water column also increases along the path (i.e., stretching of the water column), suggesting that positive relative vorticity is added to the mesoscale features due to vortex stretching.

As opposed to the cyclones, the location of the detected anticyclones (Figure 1b) and the along-strait velocity anomaly front (Figure 2f) show that the anticyclones cross Denmark Strait on the western side of the trough. The front is located between equatorward anomalies at the center of the trough and poleward anomalies on the western side (Figure 2f). The DSO direction is slightly tilted toward northwest (Figure 2h), which causes the anticyclones to slowly veer toward Greenland. The paths followed by the anticyclones suggest that the 400-m isobath prevents the anticyclones from reaching the East Greenland shelf. As the vortices move toward the shelf, the anticyclonic relative vorticity is sustained by the shrinking of the water column. When the anticyclones reach the edge of the shelf, new cyclones form south of them (Figure 3). The plots in the left column of Figure 3 show this process for a single event. The right column corresponds to composites of anticyclones detected near Station #03. First, bands of positive relative vorticity surround the slowly moving core of the anticyclones (Stage I; Figures 3a and 3b). Then, the peripheral bands of positive relative vorticity strengthen and converge, triggering the formation of cyclones south of the collapsing anticyclones (Stage II; Figures 3c and 3d). Last, the anticyclones vanish and the cyclonic features triggered by the anticyclones move southwestward following the DSO path (Stage III; Figures 3e and 3f). As these cyclones move downstream, they gain positive relative vorticity due to stretching of the water column.

3.2. Downstream Evolution of DSO Cyclones

The geometry and relative vorticity magnitude of the cyclones associated with pulses are similar to the properties of the cyclones formed during the bolus events. Therefore, to investigate their evolution as they move downstream, we created composites at fixed stations along the DSO path including all of the detected cyclones (Figure 4). The DSO stations are spaced ~20 km apart. They overlap the DSO pathway mapped by Koszalka et al. (2017) using the time- and depth-averaged trajectories of synthetic Lagrangian particles.

The background relative vorticity downstream of Denmark Strait is cyclonic along the entire DSO path (labeled circles in Figure 4a). The anticyclones associated with pulses impact the background relative vorticity, which decreases moving from the Látrabjarg Line to the Denmark Strait South station. Downstream of Station #02, where most of the anticyclones spin down, the background relative vorticity monotonically increases moving toward Station #07. This is consistent with the hypothesis that PV conservation governs the dynamics in this region (Spall & Price, 1998; von Appen et al., 2014, 2017). Positive relative vorticity is generated in response to the stretching of the water column. Downstream of Denmark Strait, the light upper layer is constrained at the surface, while the dense DSO is constrained at the bottom. As a result, the midlevel layer is stretched the most, and the relative vorticity peaks near the σ-level along which we extracted the properties of the cyclones. Downstream of Station #07, the background relative vorticity decreases as the DSO descends into the Irminger Basin, while the height of the water column continually increases from Stations #00 to #17. Therefore, PV conservation is not the dominant mechanism in the region beyond 150 km downstream of the Denmark Strait sill (past Station #07).

The composites of relative vorticity show the growth and decay phases of the DSO cyclones (black line in Figure 4a). The growth phase of the DSO cyclones occurs within the first 150 km downstream of Denmark Strait. The decay phase takes place between Station #08 and the southernmost station. Near the latter, the relative vorticity of the cyclones is similar to $\overline{f^{-1}\zeta}$ of the cyclones detected near the northernmost station. The DSO cyclones growth and decay phases are also evident in the vertical component of the velocity field (w; Figure 4b). There is a clear signal in the vertical velocities immediately before and after the detection of the cyclones (blue and red lines, respectively). Six hours before the detection of DSO cyclones, the regions occupied by the vortices are characterized by downwelling ($w < 0$). Conversely, upwelling occurs 6 hr after the detection. This characteristic behavior has been also found in the spilling events analyzed by Magaldi et al. (2011).

The Ertel PV can be approximated as follows (Klinger & Haine, 2019):

$$\mathrm{PV} \approx (f + \zeta)\frac{N^2}{g}, \tag{1}$$

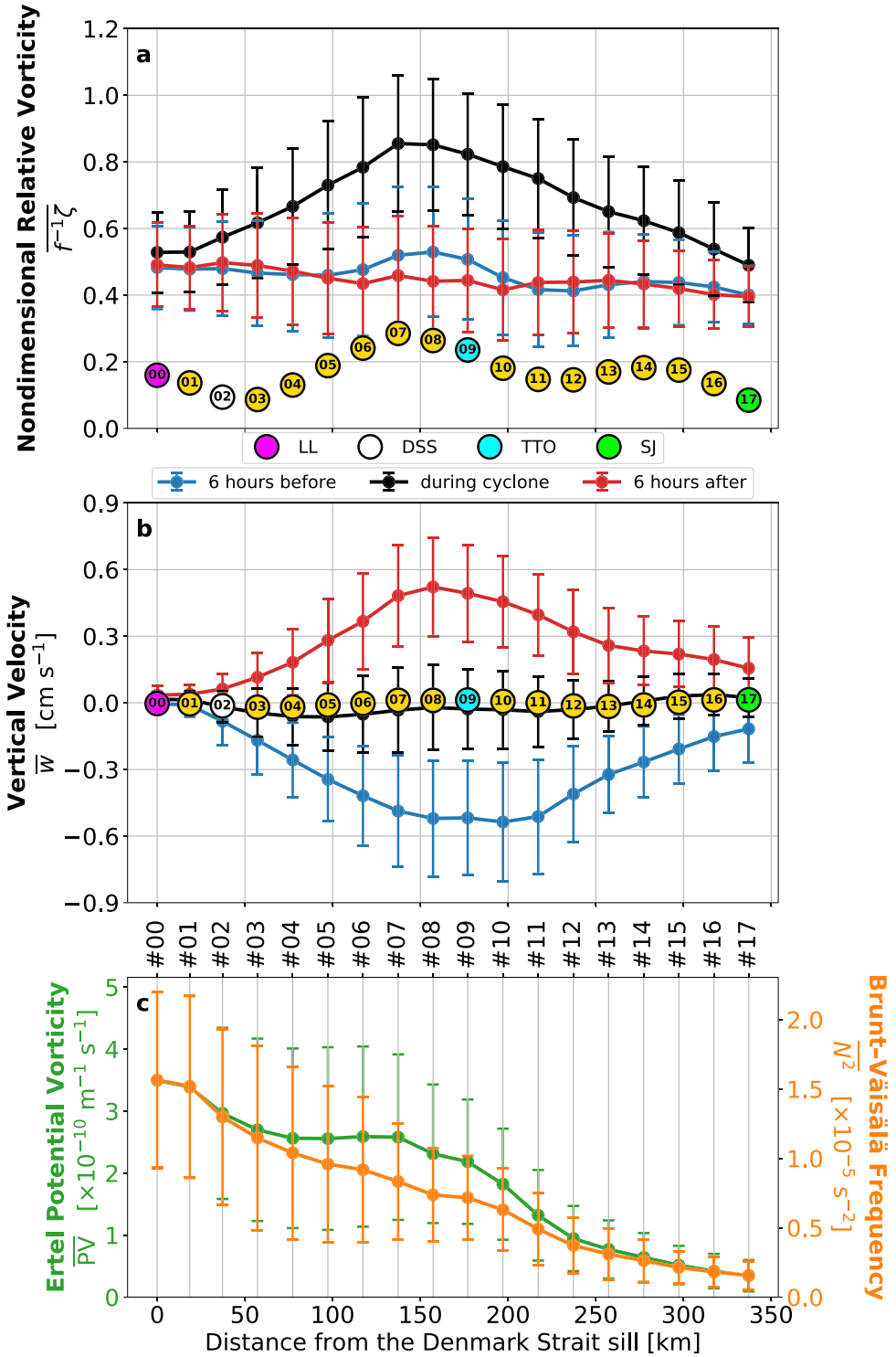

Figure 4. Composites of area-weighted mean (a) nondimensional relative vorticity, (b) vertical velocity, and (c) Ertel potential vorticity (green, left vertical axis) and Brunt-Väisälä frequency (orange, right axis) along the DSO path. Positive (negative) vertical velocities correspond to upwelling (downwelling). Lines in black (a, b) and green/orange (c) correspond to composites of DSO cyclones. Blue and red lines correspond to composites in the regions of the vortices 6 hr before and after the detection, respectively. Error bars represent the area-weighted standard deviation. Labeled circles correspond to composites of yearly averages in the regions of the vortices (background state). The color code and labeling convention of the DSO stations are the same as those used in Figure 1. Fields have been extracted along the σ-level at a depth of $5H/8$.

where N is the Brunt-Väisälä frequency, and g is the gravitational acceleration. The variability of the potential vorticity is controlled by the changes in N^2 and ζ along the DSO path. The Brunt-Väisälä frequency, which is defined by $N^2 = -\frac{g}{\rho_0}\frac{\partial \sigma_\theta}{\partial z}$, decreases as the cyclones move downstream (orange curve in Figure 4c). Therefore, the water in the midlevel layer becomes less stratified as the cyclones descend into the Irminger Basin. The potential vorticity of the DSO cyclones (green curve in Figure 4c) is strongly affected by the decrease of N^2. However, during the growth stage of the DSO cyclones (between Stations #03 and #07), the high relative vorticity of the eddies counterbalances the low stratification due to the stretching of the water column. In particular, the PV only changes by 0.12×10^{-10} m^{-1} s^{-1} in this region. It follows that, downstream of the Denmark Strait South Station (#02), the potential vorticity associated with the DSO cyclones is only conserved during the growth phase.

4. Summary and Discussion

This study focuses on mesoscale anomalies characteristic of the dense overflow descending from Denmark Strait into the Irminger Basin. We find that boluses are coupled with positive relative vorticity events, whereas pulses are coupled with anticyclonic relative vorticity events. Regardless of their initial sense of rotation, both boluses and pulses trigger the formation of DSO cyclones downstream of Denmark Strait. These findings are consistent with the one-to-one relationship between high-transport events and DSO cyclones hypothesized by von Appen et al. (2017).

The cyclonic relative vorticity associated with boluses initially increases as these features move downstream. In agreement with Spall and Price (1998) and von Appen et al. (2014), the additional positive relative vorticity gained by these mesoscale features can be explained using conservation of potential vorticity arguments. Specifically, the generation of cyclonic vorticity results from the pronounced stretching of the midlevel layer above the DSO interface, where DSO cyclones are detected. Interestingly, we find that the mechanisms controlling the formation of DSO cyclones associated with pulses are different. The along-stream direction of pulses is oriented toward Greenland compared to the orientation of boluses. As the pulses approach shallower regions, their negative relative vorticity is sustained by compression of the water column. The pulses slow down and begin to collapse near the East Greenland shelfbreak. Simultaneously, bands of positive relative vorticity surround the anticyclones. As the anticyclones weaken, the peripheral bands of positive relative vorticity strengthen and trigger the formation of DSO cyclones to the southwest. Then, the DSO cyclones associated with pulses move southward following the DSO path, and gain cyclonic relative vorticity in order to conserve their potential vorticity. Regardless of their mechanism of formation, the DSO cyclones detected are found to have similar geometry and strength.

The relative vorticity of the cyclones increases over the first 150 km downstream of the sill, then decreases. The eddies are preceded by downwelling and followed by upwelling, meaning that the leading (trailing) edge of the cyclones is directed downslope (upslope). The highest vertical velocities coincide with the peak of the cyclones' vorticity. The mean stratification of the DSO cyclones decreases during their full life cycle, while their initial increase in relative vorticity due to stretching is followed by a decrease. As a result, the growth and decay phases of the cyclones are associated with different dynamics, and potential vorticity is only materially conserved in the first 150 km downstream of Denmark Strait.

Dense overflows are ubiquitous features in the World Ocean, and our findings could apply to other regions, including the Strait of Gibraltar, the Faeroe Bank Channel, and the Strait of Sicily. An open question is why the potential vorticity associated with DSO cyclones is only conserved during their growth phase. Girton and Sanford (2003) and Voet and Quadfasel (2010) described an increase in DSO entrainment in the region where we find the transition from DSO cyclone growth to decay. In this same region, Koszalka et al. (2017) found the largest warming rate of the overflow. The decrease in potential vorticity can only be explained by diabatic and frictional processes. Therefore, these abrupt changes, combined with the enhanced entrainment and dissipation rates associated with high-transport events (i.e., boluses and pulses; North et al., 2018), might dictate which dynamics dominate the DSO cyclones' evolution at different stages of their life cycle. Further work using a combined Lagrangian-Eulerian approach is needed to fully characterize the three-dimensional structure of the DSO cyclones, and to understand how the processes discussed in this paper affect the variability downstream of our study region, between the Spill Jet section and the southern tip of Greenland.

Acknowledgments
This material is based upon work supported by the National Science Foundation under Grants OCE-1433448, OCE-1633124, OCE-1756361, and OCE-1756863. The numerical model was run on the Maryland Advanced Research Computing Center (MARCC). Marcello Magaldi helped to configure the model. OceanSpy and several packages from the Pangeo software ecosystem have been used to postprocess the model output. The numerical solutions are publicly available on SciServer (http://sciserver.org), which is developed and administered by the Institute for Data Intensive Engineering and Science at Johns Hopkins University. Instructions for accessing the data set are available at this site (https://oceanspy.readthedocs.io). Two anonymous reviewers helped to improve the content of this manuscript.

References

Almansi, M., Gelderloos, R., Haine, T. W. N., Saberi, A., & Siddiqui, A. H. (2019). OceanSpy: A Python package to facilitate ocean model data analysis and visualization. *Journal of Open Source Software*, *4*(39), 1506.

Almansi, M., Haine, T. W. N., Pickart, R. S., Magaldi, M. G., Gelderloos, R., & Mastropole, D. (2017). High-frequency variability in the circulation and hydrography of the Denmark Strait overflow from a high-resolution numerical model. *Journal of Physical Oceanography*, *47*(12), 2999–3013.

Bromwich, D. H., Wilson, A. B., Bai, L., Liu, Z., Barlage, M., Shih, C.-F., et al. (2018). The Arctic System Reanalysis, version 2. *Bulletin of the American Meteorological Society*, *99*(4), 805–828.

Bromwich, D. H., Wilson, A. B., Bai, L.-S., Moore, G. W. K., & Bauer, P. (2016). A comparison of the regional Arctic System Reanalysis and the global ERA-Interim reanalysis for the Arctic. *Quarterly Journal of the Royal Meteorological Society*, *142*(695), 644–658.

Bruce, J. G. (1995). Eddies southwest of the Denmark Strait. *Deep Sea Research Part I: Oceanographic Research Papers*, *42*(1), 13–29.

Cooper, L. (1955). Deep water movements in the North Atlantic as a link between climatic changes around Iceland and biological productivity of the English Channel and Celtic Sea. *Journal of Marine Research*, *14*(4), 347–362.

Dee, D. P., Uppala, S. M., Simmons, A. J., Berrisford, P., Poli, P., Kobayashi, S., et al. (2011). The ERA-Interim reanalysis: Configuration and performance of the data assimilation system. *Quarterly Journal of the Royal Meteorological Society*, *137*(656), 553–597.

Dickson, R. R., & Brown, J. (1994). The production of North Atlantic deep water: Sources, rates, and pathways. *Journal of Geophysical Research*, *99*(C6), 12,319–12,341.

Girton, J. B., & Sanford, T. B. (2003). Descent and modification of the overflow plume in the Denmark Strait. *Journal of Physical Oceanography*, *33*(7), 1351–1364.

Håvik, L., Almansi, M., Våge, K., & Haine, T. W. N. (2019). Atlantic-origin overflow water in the east Greenland current. *Journal of Physical Oceanography*, *49*(9), 2255–2269.

Haine, T. W. N. (2010). High-frequency fluctuations in Denmark Strait transport. *Geophysical Research Letters*, *37*, L14601. https://doi.org/10.1029/2010GL043272

Haine, T. W. N., Zhang, S., Moore, G. W. K., & Renfrew, I. A. (2009). On the impact of high-resolution, high-frequency meteorological forcing on Denmark Strait ocean circulation. *Quarterly Journal of the Royal Meteorological Society*, *135*(645), 2067–2085.

Harden, B. E., Pickart, R. S., Valdimarsson, H., Våge, K., de Steur, L., Richards, C., et al. (2016). Upstream sources of the Denmark Strait overflow: Observations from a high-resolution mooring array. *Deep Sea Research Part I: Oceanographic Research Papers*, *112*, 94–112.

Jochumsen, K., Moritz, M., Nunes, N., Quadfasel, D., Larsen, K. M. H., Hansen, B., et al. (2017). Revised transport estimates of the Denmark Strait overflow. *Journal of Geophysical Research: Oceans*, *122*(4), 3434–3450. https://doi.org/10.1002/2017JC012803

Jochumsen, K., Quadfasel, D., Valdimarsson, H., & Jónsson, S. (2012). Variability of the Denmark Strait overflow: Moored time series from 1996–2011. *Journal of Geophysical Research*, *117*, C12003. https://doi.org/10.1029/2012JC008244

Jonsson, S., & Valdimarsson, H. (2004). A new path for the Denmark Strait overflow water from the Iceland Sea to Denmark Strait. *Geophysical Research Letters*, *31*, L03305. https://doi.org/10.1029/2003GL019214

Jungclaus, J. H., Hauser, J., & Käse, R. H. (2001). Cyclogenesis in the Denmark Strait overflow plume. *Journal of Physical Oceanography*, *31*(11), 3214–3229.

Klinger, B. A., & Haine, T. W. N. (2019). *Ocean circulation in three dimensions*. Cambridge: Cambridge University Press.

Koszalka, I. M., Haine, T. W. N., & Magaldi, M. G. (2017). Mesoscale mixing of the Denmark Strait overflow in the Irminger Basin. *Ocean Modelling*, *112*, 90–98.

Krauss, W. (1996). A note on overflow eddies. *Deep Sea Research Part I: Oceanographic Research Papers*, *43*(10), 1661–1667.

Krauss, W., & Käse, R. H. (1998). Eddy formation in the Denmark Strait overflow. *Journal of Geophysical Research*, *103*(C8), 15525–15538.

Macrander, A., Käse, R. H., Send, U., Valdimarsson, H., & Jónsson, S. (2007). Spatial and temporal structure of the Denmark Strait overflow revealed by acoustic observations. *Ocean Dynamics*, *57*(2), 75–89. https://doi.org/10.1007/s10236-007-0101-x

Magaldi, M. G., Haine, T. W. N., & Pickart, R. S. (2011). On the nature and variability of the East Greenland spill jet: A case study in summer 2003. *Journal of Physical Oceanography*, *41*(12), 2307–2327.

Marshall, J., Adcroft, A., Hill, C., Perelman, L., & Heisey, C. (1997). A finite-volume, incompressible Navier Stokes model for studies of the ocean on parallel computers. *Journal of Geophysical Research*, *102*(C3), 5753–5766.

Mastropole, D., Pickart, R. S., Valdimarsson, H., Våge, K., Jochumsen, K., & Girton, J. (2017). On the hydrography of Denmark Strait. *Journal of Geophysical Research: Oceans*, *122*, 306–321. https://doi.org/10.1002/2016JC012007

Medvedev, D., Lemson, G., & Rippin, M. (2016). Sciserver compute: Bringing analysis close to the data. In *Proceedings of the 28th international conference on scientific and statistical database management*, SSDBM '16, ACM, New York, NY, USA, pp. 27:1–27:4.

Moritz, M., Jochumsen, K., North, R. P., Quadfasel, D., & Valdimarsson, H. (2019). Mesoscale eddies observed at the Denmark Strait sill. *Journal of Geophysical Research: Oceans*, *124*, 7947–7961. https://doi.org/10.1029/2019JC015273

North, R. P., Jochumsen, K., & Moritz, M. (2018). Entrainment and energy transfer variability along the descending path of the Denmark Strait overflow plume. *Journal of Geophysical Research: Oceans*, *123*, 2795–2807. https://doi.org/10.1002/2018JC013821

Okubo, A. (1970). Horizontal dispersion of floatable particles in the vicinity of velocity singularities such as convergences. *Deep Sea Research and Oceanographic Abstracts*, *17*(3), 445–454.

Reszka, M. K., Swaters, G. E., & Sutherland, B. R. (2002). Instability of abyssal currents in a continuously stratified ocean with bottom topography. *Journal of Physical Oceanography*, *32*(12), 3528–3550.

Ross, C. K. (1984). Temperature–salinity characteristics of the overflow water in Denmark Strait during overflow. *Rapports et procés-verbaux des réunions Conseil Permanent International pour l'Exploration de la Mer*, *185*, 111–119.

Semper, S., Våge, K., Pickart, R. S., Valdimarsson, H., Torres, D. J., & Jónsson, S. (2019). The emergence of the North Icelandic jet and its evolution from Northeast Iceland to Denmark Strait. *Journal of Physical Oceanography*, *49*(10), 2499–2521.

Shi, X. B., Røed, L. P., & Hackett, B. (2001). Variability of the Denmark Strait overflow: A numerical study. *Journal of Geophysical Research: Oceans*, *106*(C10), 22,277–22,294.

Spall, M. A., Pickart, R. S., Lin, P., von Appen, W.-J., Mastropole, D., Valdimarsson, H., et al. (2019). Frontogenesis and variability in Denmark Strait and its influence on overflow water. *Journal of Physical Oceanography*, *49*(7), 1889–1904.

Spall, M. A., & Price, J. F. (1998). Mesoscale variability in Denmark Strait: The PV outflow hypothesis. *Journal of Physical Oceanography*, *28*(8), 1598–1623.

Våge, K., Pickart, R. S., Spall, M. A., Moore, G. W. K., Valdimarsson, H., Torres, D. J., et al. (2013). Revised circulation scheme north of the Denmark Strait. *Deep Sea Research Part I: Oceanographic Research Papers*, *79*, 20–39.

Voet, G., & Quadfasel, D. (2010). Entrainment in the Denmark Strait overflow plume by mesoscale eddies. *Ocean Science*, *6*(1), 301–310.

von Appen, W.-J., Mastropole, D., Pickart, R. S., Valdimarsson, H., Jónsson, S., & Girton, J. B. (2017). On the nature of the mesoscale variability in Denmark Strait. *Journal of Physical Oceanography*, *47*(3), 567–582.

von Appen, W.-J., Pickart, R. S., Brink, K. H., & Haine, T. W. N. (2014). Water column structure and statistics of denmark strait overflow water cyclones. *Deep Sea Research Part I: Oceanographic Research Papers*, *84*, 110–126.

Weiss, J. (1991). The dynamics of enstrophy transfer in two-dimensional hydrodynamics. *Physica D: Nonlinear Phenomena*, *48*(2), 273–294.

Whitehead, J. A., Stern, M. E., Flierl, G. R., & Klinger, B. A. (1990). Experimental observations of baroclinic eddies on a sloping bottom. *Journal of Geophysical Research*, *95*(C6), 9585–9610.